

PAPER • OPEN ACCESS

Simulating the effects of fabrication tolerance on the performance of Josephson travelling wave parametric amplifiers

To cite this article: S Ó Peatáin et al 2023 Supercond. Sci. Technol. 36 045017

View the article online for updates and enhancements.

You may also like

- High kinetic inductance NbTiN films for quantum limited travelling wave parametric
- amplifiers
 F Mantegazzini, F Ahrens, M Borghesi et
- Balanced travelling-wave parametric amplifiers for practical applications J C Longden, J Navarro Montilla and B-K
- Non-degenerate-pump four-wave mixing kinetic inductance travelling-wave parametric amplifiers
 J C Longden and B-K Tan

Supercond. Sci. Technol. 36 (2023) 045017 (9pp)

Simulating the effects of fabrication tolerance on the performance of Josephson travelling wave parametric amplifiers

S Ó Peatáin^{1,2,*}, T Dixon^{2,3}, P J Meeson³, J M Williams², S Kafanov¹ and Yu A Pashkin^{1,*}

- ¹ Department of Physics, Lancaster University, Lancaster LA1 4YB, United Kingdom
- ² National Physical Laboratory, Teddington TW11 0LW, United Kingdom

E-mail: s.patton@lancaster.ac.uk and y.pashkin@lancaster.ac.uk

Received 23 June 2022, revised 6 February 2023 Accepted for publication 8 February 2023 Published 6 March 2023



Abstract

We present the simulated performance of a Josephson traveling wave parametric amplifier based on a one-dimensional array of radio-frequency single-junction superconducting quantum interference devices. Using the capabilities allowed by the WRspice simulation platform and previous works on this scheme, we include in our study the effects of fabrication tolerances in the device parameters on the gain of the amplifier. Our simulations show the negative effects of parameter variation and the resulting microwave reflections of signal and pump waves between individual cells. We present a method to understand the inner dynamics of the device using an impedance model that substitutes the need to simultaneously consider phase bias points and wave mixing dynamics. This should allow the application of the results presented here to more complex schemes, which promise higher amplification and fewer drawbacks. We highlight the strict limitations on parameter spread in these devices while also discussing the robustness of the scheme to defects.

Keywords: Josephson travelling wave parametric amplifier, three-wave mixing, superconductors, superconducting microwave amplifier, fabrication tolerances, parameter variation

(Some figures may appear in colour only in the online journal)

1. Introduction

Josephson tunnel junctions are ideal components for building parametric amplifiers due to their non-linear inductance and

Original Content from this work may be used under the terms of the Creative Commons Attribution 4.0 licence. Any further distribution of this work must maintain attribution to the author(s) and the title of the work, journal citation and DOI.

zero dissipation [1]. Since the first realization of the Josephson parametric amplifier (JPA) in the late 1960s [2], enormous progress has been made in the development of JPAs [3]. These amplifier schemes operated in the four-wave [2, 4–6] and three-wave [7, 8] mixing regimes, commonly referred to at that time as the four-photon and three-photon regimes (also doubly and singly degenerate modes), where the angular frequency of the signal, ω_s , the idler, ω_i , and the pump, ω_p , tones obey the relations $\omega_s + \omega_i = 2\omega_p$ and $\omega_s + \omega_i = \omega_p$, respectively.

To increase the interaction of the Josephson element with microwaves, a typical configuration of the JPA includes

³ Department of Physics, Royal Holloway University of London, Egham, Surrey TW20 0EX, United Kingdom

^{*} Authors to whom any correspondence should be addressed.

a resonant circuit coupled to the Josephson element; this imposes a limit on the amplifier's operating frequency and bandwidth set by the properties of the resonator (see, e.g. [2, 9]). To overcome this drawback, a travelling wave version of the JPA (Josephson travelling wave parametric amplifier (JTWPA)) was proposed [10] based on the analogy with the schemes used in quantum optics, where a weak signal propagates through an optical medium with non-linear polarization driven by a strong pump tone. The JTWPA consists of a large number of series-connected junctions embedded in a transmission line, which can be regarded as a one-dimensional medium composed of artificial atoms with non-linearities arising from the current-phase relation of the Josephson junction. This twoport travelling-wave structure allows for broadband transmission up to its cut-off frequency with wave impedances close to $50\,\Omega$ throughout the range. The first successful realization of the JTWPA demonstrated a gain of 16 dB and a noise temperature of 0.5 K at 1.7 K [11], well below the noise temperature of even the most advanced high electron mobility transistor amplifiers [12].

In recent years, superconducting parametric amplifier devices have seen renewed interest [13]. The greatest motivation driving this development is the necessity for detecting extremely weak signals when reading out quantum circuits [14, 15] or searching for dark matter [16]. However, considerable problems exist within current JTWPA technologies, including the cross and self-phase modulation effects, phase mismatch, pump depletion and higher-order mixing tones, each of which hampers amplifier performance [17]. To mitigate these problems, some novel designs have been proposed, including dispersion engineered devices employing resonant phase matching [15, 18, 19], periodic impedance loadings [20] and impedance modulation [21], as well as quasi-phase matching [22] and Floquet mode JTWPAs [23].

The viability of these schemes has not yet been fully considered from the point of view of fabrication tolerances and parameter spread; for this reason, we address here the question of fabrication tolerances and their effects on TWPA performance. To do this with confidence, we study the scheme first proposed [17] and further developed [22] by Zorin, which is sketched in figure 1. This scheme is chosen for its simplicity as well as for the fact that it has been studied thoroughly in previous works using the same simulation methods presented here [24]. We are confident that the lessons learned here can be applied to more complex schemes that are based on similar geometries.

The building blocks are unit cells enclosed by the dashed line in figure 1, consisting of radio-frequency single-junction superconducting quantum interference devices (rf-SQUIDs). These elements are required to provide the strong inductive non-linearity that permits parametric amplification in the 1200 cell long array where their parameters set a wavelength of ~80 nodes for a 5 GHz tone. The lumped element nature of the device and the large wavelengths in comparison with the size of individual cells allows for the application of a lumped element model [25] and simulation in lumped element circuit simulators. The application of a direct current (dc) bias or

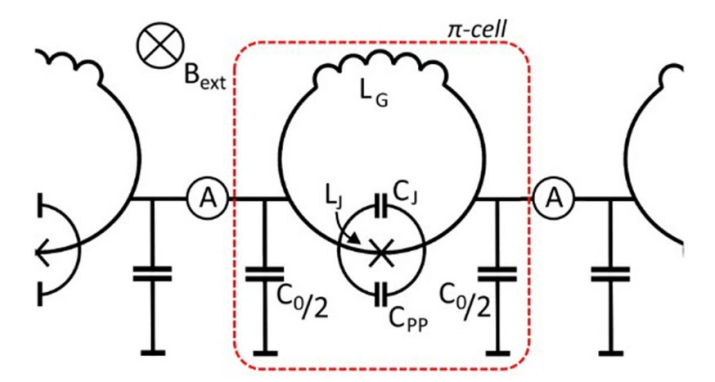


Figure 1. The π -type cell model of the transmission line under study with the rf-SQUID elements added. Geometric inductance of the loop, $L_G=57\,\mathrm{pH}$, the capacitance to ground, $C_0=100\,\mathrm{fF}$, junction, C_J , and parallel plate capacitance, C_{PP} (summing to a total junction capacitance, $C_T=60\,\mathrm{fF}$), and Josephson inductance, L_J , related to the junction critical current of $I_C=5\,\mu\mathrm{A}$, leads to a 23 Ω impedance transmission line as in Zorin's original study [17]. A single π -cell is enclosed in the dashed line, while an array of many of these can be described as an LC ladder filter. It is assumed in this model that there is no capacitive or inductive coupling between individual cells. The whole structure is placed in a uniform magnetic field denoted as B_{ext} to control the flux bias point.

an external magnetic field perpendicular to the SQUID loop plane allows for the tuning of the inductive non-linearity in the medium and operation of the amplifier in the much desired three-wave mixing regime [17]. The proposed device is estimated to offer a gain of 20 dB in the bandwidth of 5.6 GHz around a centre frequency of 6 GHz [17], although further analysis of this scheme by Dixon *et al* [24] showed that significant power is drawn to the higher harmonics, seriously hampering amplification. Using the same simulation method, we can now study the effects of variation in each of the lumped element parameters, and the effects on amplification, phase bias and amplifier stability.

With this study, we believe it should be possible for fabricators and experimentalists to have a greater understanding of the dynamics within these amplifiers and the effect of unavoidable fabrication tolerances or defects on them. We present the simulation results alongside an analytical description of the impedance characteristics of the device, which is otherwise well understood and can be readily applied to other schemes employing similar geometries and non-linear elements.

2. Mathematical model

The interlinked nature of the impedance, phase position of Josephson elements and wave mixing processes in these devices makes it all but impossible to study the effect of any of these factors in isolation. In this regard, we have chosen impedance as a key element for study due to its singular importance in the propagation of waves in the array. Therefore, phase bias and wave mixing processes can be considered only with respect to the greater picture of impedance characteristics.

For clarity, we assume that the signal and pump tones propagate from left to right in the scheme shown in figure 1. Accordingly, the cells are also numbered from left to right such that $n=0,1,2\ldots,1200$. The lumped element representation allows for the embedded rf-SQUID transmission line to be described by the π -cell model of a cascading filter or transmission line [25] shown in figure 1. This scheme and the wave mixing that occurs within can be described to a large extent by the same expressions used in the non-linear optics schemes to which it is related [17, 24, 26, 27].

In this model, the array is described as a chain of two impedances, one impedance along the direction of propagation, Z_1 , and an impedance to the return line, Z_2 . In this case, these are the impedance of the rf-SQUID and the impedance of the capacitance between the transmission line and the ground plane, respectively. This can be written in complex notation as

$$Z_1 = \frac{1}{1/(i\omega L_G) + 1/(i\omega L_J) + i\omega C_T},$$
 (1)

$$Z_2 = \frac{1}{i\omega C_0},\tag{2}$$

where $\omega=2\pi f$ and the other terms are as described in figure 1. In this way the impedance of an individual π -cell can be found to be

$$Z_{\pi} = \frac{2Z_2 \left(2Z_{\pi L}Z_2 + Z_1Z_{\pi L} + 2Z_1Z_2\right)}{4Z_{\pi L}Z_2 + 4Z_2^2 + Z_1Z_{\pi L} + 2Z_1Z_2},$$
(3)

where Z_{π} depends on $Z_{\pi L}$, the (potentially different) impedance of the preceding cell. This same geometry can be used as an impedance matching scheme due to this relation between the impedance of individual cells, and so acts over some distance to renormalize large impedance mismatches that may occur.

For $Z_{\pi} \equiv Z_{\pi L}$, and approximating that $Z_1 = i\omega L_G$ as $i\omega L_G \ll i\omega L_J$ we can simplify equation (3) to

$$Z_{\pi} = \sqrt{\frac{L_G}{C_0 \left(1 - \frac{\omega^2}{\omega_c^2}\right)}},\tag{4}$$

where the cut-off frequency of the array, ω_c , is a function of the lumped elements and is given by

$$\omega_c = \frac{2}{\sqrt{L_G(C_0 + 4C_T)}}. (5)$$

This derivation has been expanded to more fully describe the wave propagation terms in the appendix.

From equation (4) we see that when working far from the cut-off frequency, i.e. $\omega < \omega_c$, the impedance is as you would expect in a normal transmission line,

$$Z_{\pi} \approx \sqrt{\frac{L_G}{C_0}}$$
. (6)

It is evident from this that the parameters that will most greatly influence the wave impedance of the array are L_G and C_0 . The junction capacitance/parallel plate shunt capacitance should have a limited impact given the relative sizes of the impedances in this parameter set.

The variation of the junction critical currents will have a limited effect on impedance as the Josephson inductance as it is theoretically infinite under our operating conditions due to the phase biasing condition,

$$L_J = \frac{\Phi_0}{2\pi I_c} \frac{1}{\cos \varphi_{dc}},\tag{7}$$

where Φ_0 is the flux quantum, I_c is the junction critical current and φ_{dc} is the phase bias across the junction [1]. As a result, the total cell inductance $L_{\rm T}^{-1} = L_J^{-1} + L_G^{-1}$ is dominated by $L_{\rm G}$ for the optimum three-wave bias point $\varphi_{dc} = \pi/2$. However, the optimal bias point itself,

$$\varphi_{dc} + \frac{2\pi L_G I_c}{\Phi_0} \sin(\varphi_{dc}) = \frac{2\pi \Phi_{ext}}{\Phi_0},\tag{8}$$

where Φ_{ext} is the externally applied flux, may be perturbed by variations in I_c [17]. This, in turn, may impact the quadratic nonlinearity coefficient,

$$\beta = \frac{2\pi L_G I_c}{\Phi_0} \sin \varphi_{dc},\tag{9}$$

affecting the extent of the three-wave mixing [17]. Geometric inductance variation will affect phase bias and wave mixing in the same way, as will any bias phase swing that may occur during the operation of the device due, for example, to a large amplitude pump tone.

The approximation in equation (6) and other places may not be valid with a very different parameter set, such as those used in the implementation of dispersion engineering schemes. A large junction capacitance would lead to a lower cut-off frequency and greater dispersion. Divergence from this and other assumptions may create significant barriers to correct operation hampering the device's usefulness. These schemes can be analyzed in the same way as done here, but the impedance model should properly consider these added terms. In this same regard, the array must be terminated correctly to avoid any reflections from the end of the array and allow for proper power transmission [28].

Up to this point we have considered electrical parameters that can be controlled through device design. We should mention, though, that flux noise may have a significant effect on the device performance through the variation of the phase across the Josephson junctions, φ ; see equations (7)–(9). However, with proper magnetic shielding and the use of a dc bias, the flux noise can be suppressed to an insignificant level of about $1 \mu \Phi_0/Hz^{1/2}$ [29].

Other factors that can affect the phase biasing, such as optical rectification [26] and departure from the small pump approximation, will potentially affect the wave mixing dynamics in the device; however, these effects are beyond the scope of this paper.

3. Simulation

We complete our study in the same manner as in reference [24], in which the higher-order mixing dynamics of an ideal array were studied using a ladder-type model of discrete element rf-SQUIDs simulated in the WRspice program. This simulator has been proven adequate and accurate for use in Josephson circuits and JTWPAs [24, 30, 31], although it is computationally costly. This program runs a nodal analysis of the circuit in the transient evolution, solving for the current and voltage at each node of the array using Kirchoff's laws. The Josephson junction is described using the resistively and capacitively shunted junction model that can be fine-tuned to match the characteristics of physical devices [32]. In this way, we can simulate the propagation of waves through the array.

The proper flux bias for 3WM is calculated from equation (8) and inductively coupled to the geometric inductance of each rf-SQUID. The pump amplitude is set at $0.985~\mu A$ with a frequency of 12 GHz and a signal amplitude set at 5 nA with a frequency of 7.2 GHz for continuity with [24]. The resulting signal amplification is shown as the solid lines in all panels of figure 2. With the freedom provided by this simulation model we can introduce a Gaussian distribution of each of the major parameters in the design; the critical current of the junction, junction capacitance, waveguide capacitance to ground, and geometric inductance of the rf-SQUID in each π -cell of the transmission line. This allows for the investigation of variations in each parameter in isolation, with standard deviations of $\pm 1\%$, $\pm 5\%$ and $\pm 10\%$ to mimic the variation that may be expected from the various fabrication techniques [31].

Common to all systems where impedance mismatches occur, a ripple forms along the length of the waveform in the array due to complex interference between the forward and backward propagating waves encountering multiple reflections. This ripple has nodes along the length of the array for every half-wavelength period of the signal tone, while the maximum of the signal gain between nodes depends on the particular wave mixing dynamics in the array [25]. In this device, a ripple is created for all occasions of variations of parameters, which has implications on the gain and bandwidth when measuring the power output of such a device. For a robust dataset, each parameter is varied stochastically a hundred times, and the amplitude profile along the array for the ideal case of 0% variation and the envelopes of performance for each standard deviation of variation are displayed in figure 2.

As seen in equation (4), the junction capacitance has a minimal effect on the impedance of the rf-SQUID or the flux biasing point. The small impact of variation in C_J is reflected in the simulation results of figure 2(a). We note, however, that should this parameter be changed significantly for dispersion engineering or other endeavours to the point where $Z_{C_J} \sim Z_{L_G}$, then its impedance contribution is not negligible, and we can assume that variation in it would also incur a significant envelope.

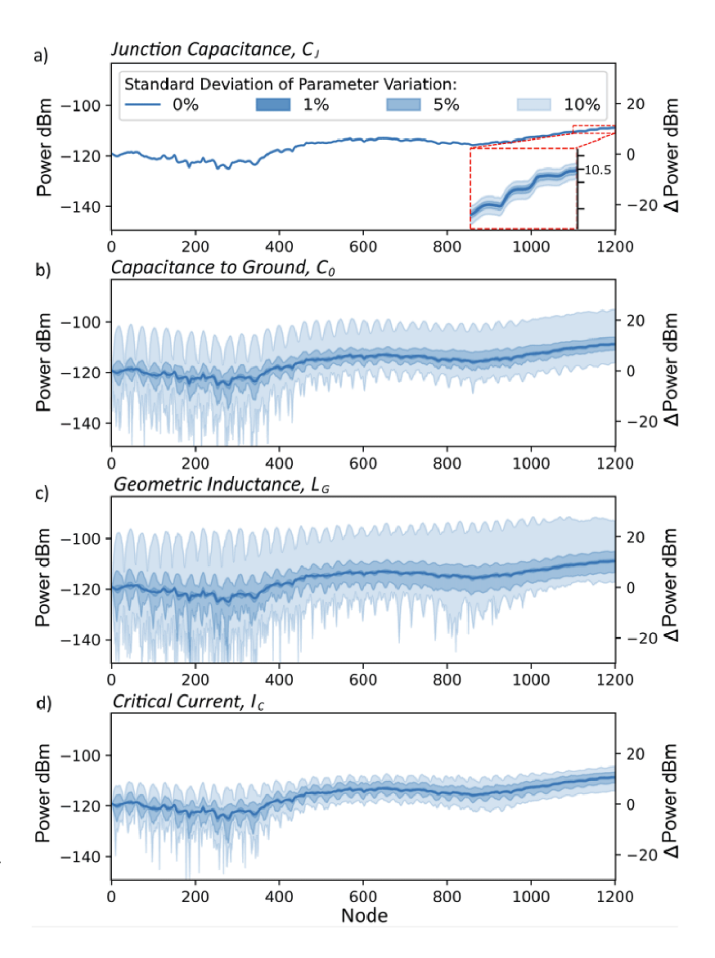


Figure 2. Envelopes of signal wave amplitude caused by variation of various parameters, where the shade of the envelope corresponds to the degree of standard deviation with the darkest at 0% standard deviation and the lightest at 10% standard deviation of the particular parameter in each unit cell. The variation in junction capacitance, C_J , (a) has very little impact on the gain profile, while the capacitance to ground, C_0 , (b) and geometric inductance, L_G , (c) create sizeable envelopes, likely due to the large effect of these parameters on array impedance. The critical current, $I_c \propto (1/L_J)$, (d) has a considerable effect but significantly less than the previous two parameters.

Furthermore, it can be expected from our impedance model that the capacitance of the transmission line to the ground plane, C_0 , and geometric inductance of the rf-SQUID loop, L_G , should have the greatest impact on device performance. This is reflected in the results, with variation in either parameter giving rise to considerable envelopes around the ideal case, as shown in figures 2(b) and (c) for each parameter, respectively. One can see that variations in these parameters of $\pm 10\%$ would produce devices with unpredictable properties, with the output gain falling in the range from almost zero up to about 25 dB.

While variations in either parameter result in a large envelope developing, primarily due to their contributions to the impedance of the device, the envelope of the geometric inductance is consistently slightly larger. This can be considered due

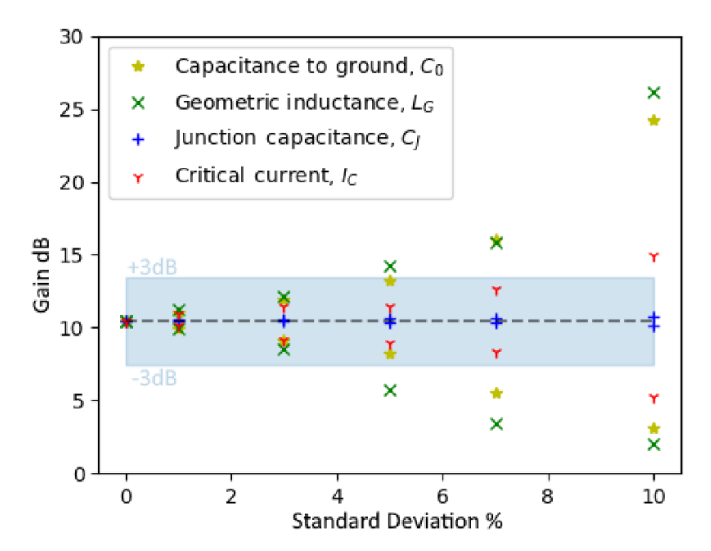


Figure 3. The bounds of the envelopes from the stochastic simulations of variation in each parameter plotted against the respective standard deviation. Standard deviations that cause variation outside of the ± 3 dB band can be considered unacceptable as this would result in a narrow or inconsistent bandwidth.

to the geometric inductance's extra contributions to the phase bias position, and as such, the impedance of the Josephson element and wave mixing properties in the array.

The fact that these parameters are the most effective is good in terms of device fabrication. The loop area can be made quite large to achieve the required inductance, making the absolute variation that may occur a smaller percentage of the whole. A similar relation applies for capacitance to ground, where a large area can be used to minimize the effects of non-uniform oxidation layers.

The variation of critical current, I_c , has been shown to have a direct effect on the wave impedance of the line via the Josephson inductance, L_J , phase bias condition and wave mixing properties. As previously stated, it is not possible to disseminate which of these effects is dominant in creating the envelopes seen for this case in figure 2(d), although the prominent ripple suggests that impedance mismatches play a large role. With the occurrence of impedance mismatch inside a group of cells, it is possible that the phase bias of the Josephson elements can be swung away from its ideal value, creating a further impedance mismatch through the Josephson inductance. Such a feedback effect may be present in this case, contributing to the creation of this large envelope.

In all cases, it can be seen that the ripple diminishes towards the end of the array, which presents as a smoothing of the envelopes in the plots of figure 2. The reason for the diminishing ripple is not fully understood, but it is thought to be due to the fact that the amplifier allows for gain in only one direction due to the application of a flux bias, and there remains a net flow of power from left to right. This, combined with the fact that there will be fewer reflection sites towards the end of the array, means that any reflected wave will appear as a smaller ripple at the end of the array as it is a smaller fraction

of the forward propagating wave at the end than it will be at the start.

The difference in the impact of variation in the individual parameters can be studied through the bounds of the individual envelopes, which is plotted in figure 3, showing a dependence of the envelope bounds on the standard deviation. We limit the useful device to output signal gain within a ± 3 dB band of the ideal device as shown by the blue shaded region.

The specific amount of variation that is tolerable to obtain a relatively flat bandwidth depends on the specific parameter set and the dominant contributions to impedance matching. However, this result shows that within some bounds ($I_c: \sigma = 8\%, C_0: \sigma = 4\%, L_G: \sigma = 3\%$) variation is tolerable for this scheme under these operating conditions.

This can be further tested through the simulation of a scheme with simultaneous variation in all parameters that is likely to occur in a realized sample. Using tolerances that can be expected from a realistic fabrication process, we set the percentage variation of each parameter for both a best and a worst case scenario, as shown in figure 4. The specific amount of random variation in parameters and any possible systematic or gradiometric variations across the chip depend greatly on the fabrication method used [31, 33], and are outside the scope of this study.

The envelopes make it clear that the performance gets significantly worse with all the added variations. However, the situation is reasonable with an optimal fabrication method, and the gain of the amplifier at the final node is expected to be 10 ± 2 dB. However, in the worst case studied the situation is considerably less promising with a final node gain of 10^{+20}_{-10} dB. This translates to an unpredictable gain in samples fabricated with such tolerances.

It may be tempting to see possible silver linings to these variations in that larger amplification can be seen in some conditions, as shown in the case of two individual results taken from the make-up of the worst case envelope in figure 4(b). This is shown in the bandwidth plot of these individual cases in figure 5, where two spikes emerge for the case of a ripple resulting in a very high gain reaching 30 dB at 7.2 GHz (orange curves of figures 4(b) and 5). However, this effect is constrained to a specific signal frequency range, likely due to some sort of resonance forming in the array. Such a device cannot be considered stable [28, 34] and so generating high gain through these instabilities is impractical for a robust and reliable broadband amplifier. Aside from these instabilities, a ripple develops across the frequency response for both cases with variation, which can also make an amplifier more difficult to use in practice.

However, it should be noted that the device performance over the full frequency range for either of the cases with ripples does not differ too greatly from the ideal case with no variation, with the exception of the two obvious peaks.

With modern fabrication techniques, the variation that can be expected in the most consequential parameters like geometric inductance (loop area) can be kept low, although with angle deposition this will depend greatly on the design. Variation in

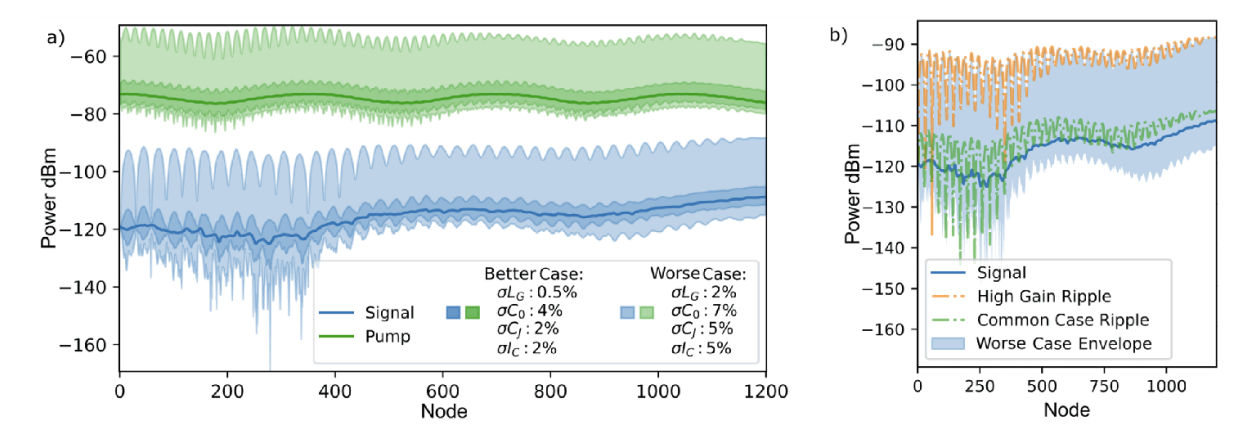


Figure 4. (a) Combined effect of variation of geometric inductance, capacitance to ground, junction capacitance and critical current, on the performance of the device, with envelopes forming around both the signal and pump tones. Variations in impedance or proper biasing can seriously affect performance, even in the best possible case. (b) Two singular examples of the simulation results taken from the worst case simulations are shown in their respective places in the envelope. The larger ripple (orange) and smaller ripple (green) are examples of the unpredictable effects that variation may have, with significantly higher gain possible under some conditions.

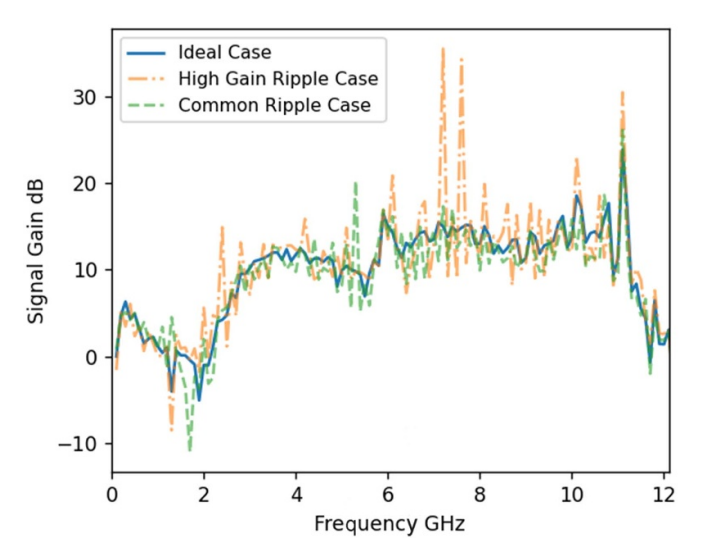


Figure 5. Plot of gain against signal tone frequency for a signal tone of 5 nA and a pump tone of $0.985 \,\mu\text{A}$ at 12 GHz. The orange and green curves correspond to the parameter sets that create the similarly coloured curves in figure 4(b), while the solid line is the ideal case of no variations.

oxidation across the array's junctions and capacitances may not be so damning, despite this aspect of the design seeing the greatest standardization efforts. This should allow for the fabrication of functional devices if designers and fabricators examine the parameters most consequential in their scheme. It is still possible that the variation that is natural to even the best techniques will result in aberrant behaviour at specific frequencies; however, the device may behave well aside from this, as seen in figure 5.

Another common problem that may arise in fabrication is localized defects, including shorts along the line to the ground plane, broken inductive loops, or shorted junctions. Very different effects can be seen depending on the specific placement of the defect.

For defects that occur in the impedances to the return line of the π -cell model, such as a short in the ground capacitor

in this scheme, a step-like impedance mismatch occurs, leading to almost total reflection of the wave from that point. Meanwhile, a defect within the rf-SQUID that does not completely break the loop on both sides, such as the common defect of a shorted junction, will not have such a damaging effect. An impedance mismatch certainly occurs but not to such a large degree as in the previous example, so with several shorted junctions along the array a ripple develops but the device is still in a useful condition. Both of these situations are shown in figures 6(a) and (b), respectively, where the defects are added at certain points in the array marked by the vertical dashed lines. This result can likely be extended to unit cells of similar geometry that use Josephson tunnel junctions, showing that these amplifiers are fortunately quite robust to the most common of the localized defects studied.

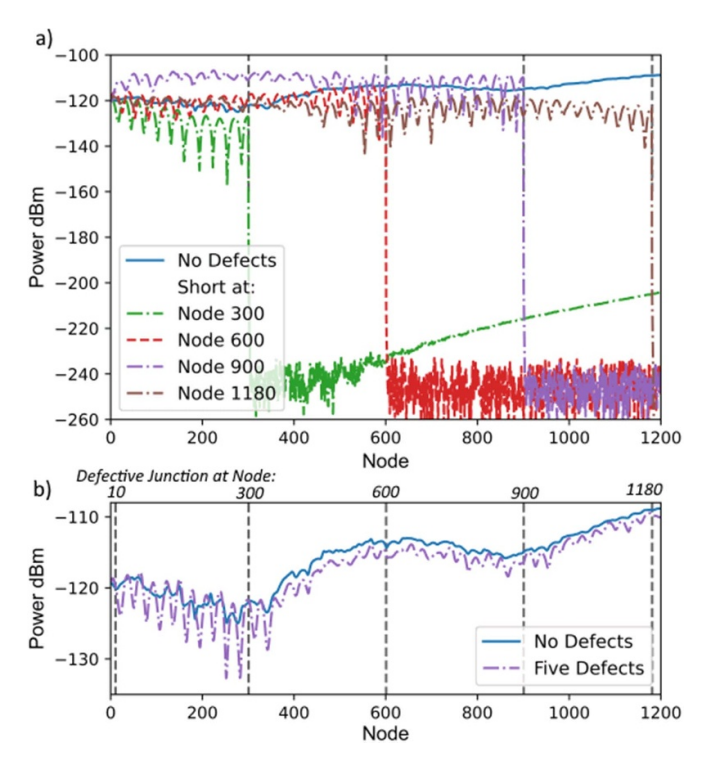


Figure 6. Effect of point defects on the amplifier performance. (a) Shorts to ground due to broken C_0 at multiple locations along the line causing boundary reflections, and the associated ripple prior to the short and attenuation of the signal to the simulation noise floor following the short. (b) A short across the Josephson junction is added at various points along the array. It is shown that the tones continue to propagate, but a significant impedance mismatch causes reflections from these points and a ripple forms along the gain curve.

4. Conclusion

We have completed a quantitative analysis of the effect of random parameter variations within the SQUID array amplifier proposed recently [17]. Through systematic treatment of parameter variations and the development of an impedance model for the amplifier scheme, we have gained an insight into the system. A parameter's contribution to the impedance of an individual cell has been identified as the greatest factor determining what effect fabrication tolerances in the said parameter will have on the device performance. Consequently, the geometric inductance of the rf-SQUID loops and the capacitance of the transmission line to ground were found to have the greatest impact on gain, primarily due to their contributions to the impedance in this scheme. Furthermore, geometric inductance was seen to have a slightly larger effect, likely due to its extra contributions in setting the Josephson junction flux bias and impedance. Fortunately, both of these parameters can be controlled fairly well with the right fabrication and design methods, resulting in low variation of either parameter by increasing the area of the inductive loops and capacitive pads, respectively.

With this information and the relations provided, it should be possible for fabricators and experimentalists to better understand the inner dynamics of other Josephson travelling wave-type amplifier schemes to which these results can readily be applied.

We have also shown that certain defects that occur within the rf-SQUID are not terminal but can compound if they occur in quantity, diminishing the device performance. This shows that amplifier designs involving SQUIDs of any kind are remarkably robust to defects that one may have otherwise thought terminal. However, if a capacitance to ground becomes shorted, the entirety of the signal will likely be reflected from the defect.

We have also studied the maximum fabrication tolerances that can be present in such a device that will ensure the gain to be within a $\pm 3\,\mathrm{dB}$ corridor. Thus, with state-of-the-art fabrication facilities, the rf-SQUID-embedded JTWPA is a strong candidate for broadband, high-gain, high-yield parametric amplifiers. Our approach to the analysis of the parameter variation on the JTWPA performance is not limited to this scheme alone. Such an analysis would give greater confidence in predicting the behaviour of as-yet unrealized devices or many more complex amplifier designs and other 1D metamaterials, such as kinetic inductance TWPAs.

Data availability statement

Due to the prohibitive size of the dataset we are unable to host online publicly, but are happy to share the data with interested parties. The data that support the findings of this study are available upon reasonable request from the authors.

Acknowledgment

We thank C Kissling, R Dolata and A B Zorin for their fruitful discussions and useful comments. This work was partially funded by the Joint Research Project 17FUN10 ParaWave of the EMPIR Programme, co-financed by the Participating States and from the European Union's Horizon 2020 research and innovation programme. We acknowledge support from the QSHS project ST/T006102/1 funded by STFC.

Appendix. Derivation of impedance characteristics

The following derivation is reproduced with some extra steps from 'Network Analysis and Practice' - Walton [25] for clarity on the derivation of wave propagation characteristics in the device.

The characteristic impedance of an infinite chain of impedances Z_1 and Z_2 can be calculated using a π -cell model, where the impedance to ground, Z_2 , is split equally between neighbouring cells as shown in figure A1. The following derivation can be repeated for other cases as shown in [25]. A π -cell added to the end of the infinite chain has its impedance, Z_{π} , calculated from the impedance network as

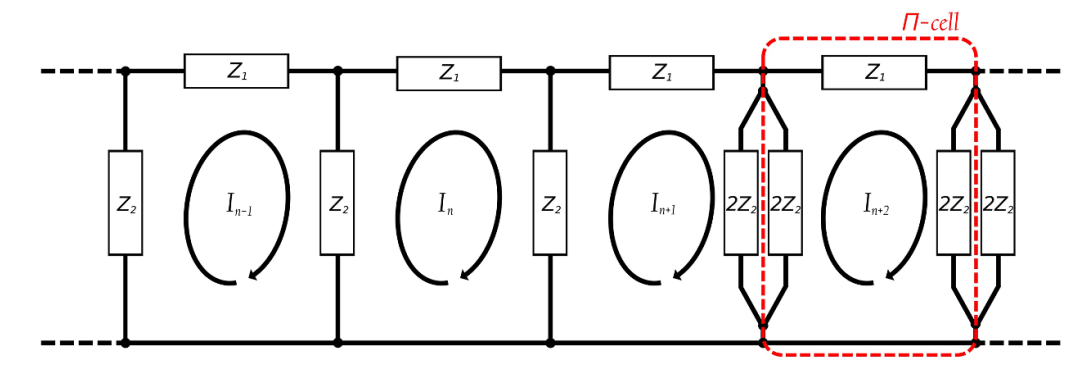


Figure A1. An infinite chain of impedances Z_1 along the direction of propagation and Z_2 to ground that can be described as a transmission line and examined using the π -cell model, where the impedance Z_2 is split equally between neighbouring cells.

$$Z_{\pi}^{-1} = \begin{bmatrix} \left(\frac{2Z_{\pi L}Z_2}{Z_{\pi L} + 2Z_2}\right) + Z_1 \end{bmatrix}^{-1} + [2Z_2]^{-1}, \qquad (A.1) \qquad \text{This leads to a transfer function, } \mathscr{T}, \text{ in terms of } I_n \text{ and } I_{n+1}, \\ \text{such that}$$

$$Z_{\pi} = \frac{2Z_{2}[Z_{1}Z_{\pi L} + 2Z_{1}Z_{2} + 2Z_{2}Z_{\pi L}]}{2Z_{2}[2Z_{\pi L} + Z_{1} + 2Z_{2}] + Z_{1}Z_{\pi L}},$$
 (A.2)

where $Z_{\pi L}$ is the impedance of the preceding cell that loads it. Assuming that each cell is equally loaded, i.e. that $Z_{\pi} \equiv Z_{\pi L}$, this equation is reduced to

$$Z_{\pi} = \sqrt{\frac{Z_1 Z_2}{1 + Z_1 / 4 Z_2}}. (A.3)$$

 Z_{π} is imaginary when the denominator of the above equation is negative, meaning waves cannot propagate. Therefore, at $Z_1/4Z_2 = -1$, a critical frequency for wave propagation, ω_c , can be determined.

Writing impedances Z_1 and Z_2 in terms of the reactances used in the TWPA circuit, (2), we come to

$$\frac{Z_1}{4Z_2} \equiv \frac{\omega_c C_0 L_G/C_J}{4\omega_c L_G - 4/\omega_c C_J} = -1, \tag{A.4} \label{eq:A.4}$$

and

$$\omega_{\rm c} = \frac{2}{\sqrt{L_{\rm G}(C_0 + 4C_{\rm I})}}.$$
 (A.5)

Therefore, rewriting Z_{π} in terms of ω_{c} ,

$$Z_{\pi} = \sqrt{\frac{L_{G}}{C_{0} (1 - \omega^{2} / \omega_{c}^{2})}}. \tag{A.6}$$

To better understand the wave propagation and dispersion in the device, the transfer equation between cells must be found. Looking at the current flows in the (n+1)th cell of the chain shown in figure A1, we find

$$\left[Z_2 + Z_1 + \frac{2Z_2Z_{\pi}}{2Z_2 + Z_{\pi}}\right]I_{n+1} = Z_2I_n. \tag{A.7}$$

$$\mathscr{T}^{-1} = \frac{I_n}{I_{n+1}} \equiv \frac{Z_2 + Z_1 + \frac{2Z_2Z_{\pi}}{2Z_2 + Z_{\pi}}}{Z_2}, \tag{A.8}$$

$$\mathscr{T}^{-1} = \frac{Z_2(2Z_1 + 2Z_2 + 3Z_{\pi}) + Z_1Z_{\pi}}{2Z_2^2 + Z_2Z_{\pi}}.$$
 (A.9)

Using (A.3) and for convenience writing $Z_1/4Z_2$ as u, we can rewrite the above as

$$\mathscr{T}^{-1} = 1 + \frac{Z_1}{Z_2} + \frac{2\sqrt{Z_1Z_2}}{2Z_2\sqrt{1+u} + \sqrt{Z_1Z_2}},$$
 (A.10)

$$\Rightarrow \frac{2\sqrt{Z_{1}Z_{2}}\left(2Z_{2}\sqrt{1+u}-\sqrt{Z_{1}Z_{2}}\right)}{4Z_{2}^{2}(1+u)-Z_{1}Z_{2}},\tag{A.11}$$

$$\Rightarrow \frac{2\sqrt{Z_1Z_2}\sqrt{1+u}-Z_1}{2Z_2}, \tag{A.12}$$

$$\mathcal{T}^{-1} = 1 + \frac{Z_1}{2Z_2} + \sqrt{\frac{Z_1}{Z_2}(1+u)}.$$
 (A.13)

The relation between the transfer function and propagation constant, γ , allows us to expand the relation:

$$\mathcal{T} = \exp(-\gamma) = \left[1 + 2u + \sqrt{4u(1+u)}\right]^{-1},$$
 (A.14)

$$\cosh \gamma = \frac{1}{2} \left(\mathscr{T} + \mathscr{T}^{-1} \right), \tag{A.15}$$

$$\Rightarrow \frac{1}{2} \left[\frac{\left(1 + 2u + \sqrt{4u(1+u)}\right)^2 + 1}{1 + 2u + \sqrt{4u(1+u)}} \right] \times \left[\frac{1 + 2u - \sqrt{4u(1+u)}}{1 + 2u - \sqrt{4u(1+u)}} \right], \quad (A.16)$$

$$\Rightarrow 1 + 2u. \tag{A.17}$$

Expanding the propagation constant into its constituent parts of attenuation, α , and phase shift, β , constants,

$$\cosh \gamma = \cosh (\alpha + i\beta) = 1 + 2u \tag{A.18}$$

$$= \cosh \alpha \cos \beta + i \sinh \alpha \sin \beta \qquad (A.19)$$

and using the assumption of lossless transmission, i.e. $\alpha = 0$, and the relation for the wavevector, $k = i\gamma$, we can find a simple relation for the dispersion relation of waves propagating along the chain:

$$k = \arccos\left(1 + \frac{Z_1}{2Z_2}\right),\tag{A.20}$$

or using the small-angle approximation,

$$k = 1 + \frac{\omega C_0 L_G / C_J}{2\omega L_G - 2/\omega C_J}.$$
 (A.21)

While the specific reactances may change, this method is broadly applicable to similar schemes, making it useful in characterizing travelling wave parametric amplifier schemes.

ORCID iDs

S Ó Peatáin https://orcid.org/0000-0001-5563-9301 Yu A Pashkin https://orcid.org/0000-0003-4767-8217

References

- [1] Barone A and Paterno G 1982 *Physics and Applications of the Josephson Effect* (New York: Wiley)
- [2] Zimmer H 1967 Parametric amplification of microwaves in superconducting Josephson tunnel junctions Appl. Phys. Lett. 10 193
- [3] Pedersen N F 2019 RF Applications of Superconducting Tunneling Devices (Berlin: De Gruyter) pp 739–62
- [4] Parrish P T and Chiao R Y 1974 Appl. Phys. Lett. 25 627-9
- [5] Feldman M J, Parrish P T and Chiao R Y 1975 J. Appl. Phys. 46 4031–42
- [6] Wahlsten S, Rudner S and Claeson T 1977 Appl. Phys. Lett. 30 298–300
- [7] Kanter H and Silver A H 1971 Appl. Phys. Lett. 19 515-7
- [8] Mygind J, Pedersen N F and Soerensen O H 1978 Appl. Phys. Lett. 32 70–2
- [9] Hatridge M, Vijay R, Slichter D H, Clarke J and Siddiqi I 2011 Phys. Rev. B 83 134501
- [10] Sweeny M and Mahler R 1985 IEEE Trans. Magn. 21 654

- [11] Yurke B, Roukes M L, Movshovich R and Pargellis A N 1996 Appl. Phys. Lett. 69 3078
- [12] Low Noise Factory 2018 LNF- 4–16 GHz cryogenic low noise amplifier (available at: www.lownoisefactory.com/files/ 3615/2585/7568/LNF-LNC4_16B.pdf)
- [13] Aumentado J 2020 IEEE Microw. Mag. 21 45-59
- [14] Bultink C C, Tarasinski B, Haandbæk N, Poletto S, Haider N, Michalak D J, Bruno A and DiCarlo L 2018 Appl. Phys. Lett. 112 092601
- [15] Macklin C, O'Brien K, Hover D, Schwartz M E, Bolkhovsky V, Zhang X, Oliver W D and Siddiqi I 2015 Science 350 307–10
- [16] Brubaker B M et al 2017 Phys. Rev. Lett. 118 061302
- [17] Zorin A B 2016 Phys. Rev. Appl. 6 034006
- [18] O'Brien K, Macklin C, Siddiqi I and Zhang X 2014 Phys. Rev. Lett. 113 157001
- [19] White T C et al 2015 Appl. Phys. Lett. 106 242601
- [20] Vissers M R, Erickson R P, Ku H S, Vale L, Wu X, Hilton G C and Pappas D P 2016 Appl. Phys. Lett. 108 012601
- [21] Ranadive A, Esposito M, Planat L, Bonet E, Naud C, Buisson O, Guichard W and Roch N 2022 Nat. Commun. 13 1737
- [22] Zorin A B 2021 Appl. Phys. Lett. 118 222601
- [23] Peng K, Naghiloo M, Wang J, Cunningham G D, Ye Y and O'Brien K P 2021 Near-ideal quantum efficiency with a floquet mode traveling wave parametric amplifier (arXiv:2104.08269)
- [24] Dixon T, Dunstan J W, Long G B, Williams J M, Meeson P J and Shelly C D 2020 Phys. Rev. Appl. 14 034058
- [25] Walton A K 1987 Network Analysis and Practice (Cambridge: Cambridge University Press)
- [26] Boyd R W 2020 The nonlinear optical susceptibility Nonlinear Optics 4th edn, ed R W Boyd (New York: Academic) ch 1, pp 1–64
- [27] Yaakobi O, Friedland L, Macklin C and Siddiqi I 2013 Phys. Rev. B 87 144301
- [28] Planat L, Ranadive A, Dassonneville R, Puertas Martínez J, Léger S, Naud C, Buisson O, Hasch-Guichard W, Basko D M and Roch N 2020 Phys. Rev. X 10 021021
- [29] Jabdaraghi R N, Golubev D S, Pekola J P and Peltonen J T 2017 Sci. Rep. 7 8011
- [30] Shelly C D, See P, Romans E J, Casaburi A, Ireland J, Williams J M and Hadfield R H 2017 Modelling of a two-signal SFQ detection scheme for the readout of superconducting nanowire single photon detectors 16th Int. Superconductive Electronics Conf. (ISEC) pp 1–3
- [31] Naaman O, Ferguson D G, Marakov A, Khalil M, Koehl W F and Epstein R J 2019 High saturation power Josephson parametric amplifier with GHz bandwidth 2019 IEEE MTT-S Int. Microw. Symp. (IMS) pp 259–62
- [32] Whiteley S 1991 *IEEE Trans. Magn.* 27 2902–5
- [33] Dolata R, Scherer H, Zorin A B and Niemeyer J 2005 J. Appl. Phys. 97 054501
- [34] Macklin C 2015 PhD Thesis UC Berkeley